第31卷第2期
2012年4月

红外与毫米波学报
J. Infrared Millim. Waves

Vol. 31, No. 2
April, 2012

文章编号:1001 - 9014(2012)02 - 0097 - 06

Spin polarized transport through double quantum dots embedded in A-B ring coupled to ferromagnetic leads

WANG Wu-Tao, XIN Zi-Hua, CHEN Si-Lun
(Department of Physics, Shanghai University, Shanghai 200444, China)

Abstract: The spin polarized transport through double quantum dots embedded in one arm of an A-B ring coupled to ferromagnetic leads has been studied in this paper. The Keldysh nonequilibrium Green function method is used to calculate the total tunneling current, the spin up current, the spin down current and the spin accumulation. The magnitude of them can be modulated by adjusting the polarization, the bias voltage and the magnetic flux in parallel and antiparallel configuration. With the spin-polarization strength P increasing, the total tunneling current decreases in both parallel and antiparallel configuration, and the tunneling for spin up and spin down electrons are different in two configurations. By tuning the magnetic flux, obvious interference between the two different paths can be observed. The spin accumulation in both QDs in antiparallel configuration is also investigated, and increases with the increase of P.

Key words: ferromagnetic electrodes; quantum dots; A-B ring
PACS: 72.25. - b, 73.63. Kv, 85.35. Ds

两端联有铁磁电极的 A-B 环中的双量子点自旋极化输运

王吴韬, 辛子华, 陈思伦
(上海大学 物理系,上海 200444)

摘要:运用 Keldysh 格林函数方法,研究了两端联有铁磁电极的 A-B 环中的双量子点自旋极化输运.研究结果显示,系统的隧穿电流、自旋向上电流、自旋向下电流以及自旋累积明显的受自旋极化强度、外加电压和磁通的影响,并且随着极化强度的增大,在平行与反平行组态下的隧穿电流都减小,另外还出现了自旋分流现象.通过改变磁通,能明显地观察到两条通道的干涉现象.反平行组态下的自旋累积会随着极化强度的增大而增大.

关 键 词:铁磁电极;量子点;A-B 环
中图分类号:0469 **文献标识码**:A

Introduction

The spin-based devices, which utilize the spin other than the charge of an electron, have been intensively studied in recent years, from both the experimental and the theoretical points of view[1-5]. Due to its potential applications in spintronics and quantum computing, spin-polarized transport in quantum dots coupled to ferromagnetic electrodes has attracted much interest. Sergueev et al[6] studied the transport characteristics of a spin-valve system formed by a quantum dot coupled to two ferromagnetic electrodes whose magnetic moments are oriented at an angle θ, and found that the Kondo peaks in the local density of states and in the conductance can be modulated by θ. Then, many works mainly focus on the spin-polarized transportation in the magnetic nanostructure consisting of one quantum dot or double quantum dots have been done to investigated the Kondo effect, the Coulomb blockade effect, the tunnel magnetoresistance (TMR) and so on.

In addition, an Aharnov-Bohm (AB) ring de-

Received date: 2011 - 03 - 19, **revised date**: 2011 - 12 - 24 **收稿日期**:2011 - 03 - 19, **修回日期**:2011 - 12 - 24
Foundation items: Shanghai Leading Academic Discipline Project(S30105)
Biography: WANG Wu-Tao(1986-), male, Jiangsu Province, master candidate. Research on spin polarized transport in quantum dots system. E-mail: wangwutao@ shu. edu. cn.

vice, in which one or two quantum dots are located in its arms, has also attracted much interest[7-9]. B. Dong *et al.* [7] have studied the quantum transport through a parallel double-dot system with the Aharonov-Bohm magnetic flux infiltering the two path closed region. They found that the external bias voltage induced superposition of two dot states is the cause of phase coherence of AB oscillations of population of each dot and the current as a function of magnetic flux having a period of Φ_0.

However, previous work has paid little attention to the investigation of the spin-polarized transport in a magnetic nanostructure with two quantum dots embedded in one path of an A-B ring couple to ferromagnetic electrodes, so the motivation of this paper, is to investigate the spin-polarized transport in such a system.

1 Model and theory

The model system under consideration is illustrated in Fig. 1. It consists of two ferromagnetic leads coupled to an AB ring with two dots embedded in one path. For simplicity, magnetic moments of the leads are assumed to be either parallel or antiparallel. Here we focus our investigation on the spin-polarized transport through this system where the magnetic flux penetrates.

The system of a mesoscopic ring with a two-QD molecule can be described by the Hamiltonian

$$H = H_{\text{leads}} + H_d + H_T \quad , \tag{1}$$

$$H_{\text{leads}} = \sum_{k\alpha\sigma} \varepsilon_{k\alpha} c^+_{k\alpha\sigma} c_{k\alpha\sigma} \quad , \tag{2}$$

$$H_d = \sum_{i\sigma} (\varepsilon_i d^+_{i\sigma} d_{i\sigma} + U n_{i\sigma} n_{i\bar{\sigma}}) \quad , \tag{3}$$

$$H_T = \sum_{k\sigma} (t_{Ld1} c^+_{kL\sigma} d_{1\sigma} + t_{Rd2} c^+_{kR\sigma} d_{2\sigma} + H.c) + \sum_{k\alpha} (t_{LR} e^{-i\phi} c^+_{kL\sigma} c_{kR\sigma} + H.c) + \sum_{\sigma} (t_{d1d2} d^+_{1\sigma} d_{2\sigma} + H.c) \quad , \tag{4}$$

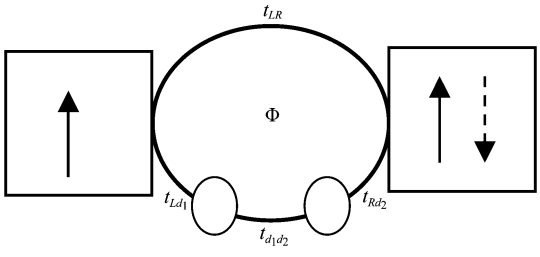

Fig. 1 Scheme of double quantum dots embedded in one arm of an Aharnov-Bohm ring coupled to ferromagnetic electrodes
图1 两端联有铁磁电极的A-B环中的双量子点系统

where $c^+_{k\alpha\sigma}$ ($c_{k\alpha\sigma}$) are the electron creation (annihilation) operators in lead α ($\alpha = \text{L}, \text{R}$) with momentum k, spin σ ($\sigma = \uparrow, \downarrow$, or $\sigma = \pm 1$) and energy $\varepsilon_{k\alpha}$. $d^+_{i\sigma}$ ($d_{i\sigma}$) creates (annihilates) an electron with spin σ on the i th ($i = 1, 2$) dot. Each QD consists of a single level ε_i and an on-site Coulomb repulsion with constant strength U. t_{d1d2} describes the interdot coupling between QD1 and QD2, while the coupling between QD1 (QD2) and the left (right) lead is represented by t_{Ld1} (t_{Rd2}). t_{LR} describes the direct tunneling between two leads. Considering the existence of magnetic flux Φ penetrating in the ring, a phase factor $\phi = 2\pi\Phi/\Phi_0$ generates in the tunneling coupling term t_{LR}.

Through the Keldysh nonequilibrium Green's function technique, we could analyze the quantum transport property of this device. The current of each spin component flowing from the left lead into the ring can be written as

$$I_{L\sigma} = \frac{2e}{\hbar} \int \frac{d\omega}{2\pi} \text{Re}[t_{Ld1} G^<_{d1L\sigma} + t_{LR} e^{-i\phi} G^<_{RL\sigma}] \quad . \tag{5}$$

The lesser Green functions can be obtained straightforwardly by using the standard Keldysh equation

$$G^<_\sigma = G^r_\sigma g^{r-1}_\sigma g^<_\sigma g^{a-1}_\sigma G^a_\sigma + G^r_\sigma \sum\nolimits^<_\sigma G^a_\sigma \quad , \tag{6}$$

where the first and the second term describes the elastic and the inelastic transport, respectively. In our present case, we only consider the elastic transport, so we can simply take $\sum^<_\sigma = 0$ [10,11]. $g^{r-1}_\sigma g^<_\sigma g^{a-1}_\sigma$ is diagonal, with only two nonzero matrix elements $g^{r-1}_{\alpha\alpha\sigma} g^<_{\alpha\alpha\sigma} g^{a-1}_{\alpha\alpha\sigma} = 2if_\alpha(\omega)/\pi\rho_{\alpha\sigma}$, where $f_\alpha(\omega) = \{\exp[(\omega - \mu_\alpha)/k_BT] + 1\}^{-1}$ is the Fermi distribution function for lead α with chemical potential μ_α.

In order to obtain the lesser Green's functions, the retarded Green's functions can be worked out by the Dyson equation $G^r_\sigma = g^r_\sigma + g^r_\sigma \sum\nolimits^r_\sigma G^r_\sigma$. The bare Green's functions g^r_σ in the leads are taken in the form $g^r_{\alpha\alpha\sigma} = -i\pi\rho_{\alpha\sigma}$.

By the equation of motion method, $g^r_{d_id_i\sigma}$ on the dots can be written as $g^r_{d_id_i\sigma} = \dfrac{\omega - \varepsilon_i - U + Un_{i\bar{\sigma}}}{(\omega - \varepsilon_i)(\omega - \varepsilon_i - U)}$, $(i = 1, 2)$. $n_{i\bar{\sigma}}$ is the electron occupation number with spin $\bar{\sigma}$ on the i th dot, and can be determined self-consistently by the equation

$n_{i\bar{\sigma}} = -i\int \frac{d\omega}{2\pi} G^{<}_{d_i d_i \bar{\sigma}}(\omega)$. By neglecting higher-order terms, the retarded self-energy $\sum_{\sigma}^{r}$ is composed of elements which denote the dot-lead and the lead-lead tunneling coupling strengths. In addition, the spin accumulation is defined as $\Delta n_i = n_{i\uparrow} - n_{i\downarrow}$.

2 Results and discussion

In numerical calculation we set $t_{Ld1} = t_{Rd2} = 0.4$, $t_{LR} = 0.1$ and $t_{d_1 d_2} = 0.8$. The temperature is set to $k_B T = 0.01$ throughout the paper. In the wideband limit, we can neglect the energy dependence in $\Gamma_{\alpha\sigma}$, which can be taken in the form $\Gamma_{\alpha\sigma} = 2\pi\rho_{\alpha\sigma}|t_{\alpha d_i}|^2$, and the effective spin-polarization strength P is written as $P = (\Gamma_{\alpha\sigma} - \Gamma_{\alpha\bar{\sigma}})/(\Gamma_{\alpha\sigma} + \Gamma_{\alpha\bar{\sigma}})$. From the definition of P, $\Gamma_{\alpha\sigma}$ can be expressed as $\Gamma_{L\uparrow} = \Gamma_{R\uparrow} = \Gamma_0(1+P)$, $\Gamma_{L\downarrow} = \Gamma_{R\downarrow} = \Gamma_0(1-P)$ for the parallel configuration, and $\Gamma_{L\uparrow} = \Gamma_{R\downarrow} = \Gamma_0(1+P)$, $\Gamma_{L\downarrow} = \Gamma_{R\uparrow} = \Gamma_0(1-P)$ for the antiparallel configuration. Γ_0 describes the coupling between the QD and leads without internal magnetization, and is expressed as $\Gamma_0 = 2\pi\rho_0 t^2_{\alpha d_i} \approx 1$. ρ_0 is the local density of states in the leads without internal magnetization, and is set to $\rho_0 = 1$. The chemical potentials of the left and right leads are $\mu_L = -\mu_R = \frac{V}{2}$.

Fig. 2 shows the bias dependence of tunneling current in parallel and antiparallel configurations for different polarization strength P. From this figure one can see that, when the bias voltage V changes, the tunneling current reveal steplike characteristics as well as that in one QD system. These results are ascribed to the Coulomb blockade effect. Due to the Coulomb blockade effect, both the spin-up and spin-down current should present the steplike features for electron transport through the parallel and antiparallel configurations. When $V = 0$, no tunneling currents appear in both configurations, which means no spontaneous current exists in such systems. It is also found that the values of the current are different at different polarization P of the leads, and the magnitude of current in both configurations decrease with P increasing. When $P = 0$, the tunneling current in both configurations are identical, because the contribution of electrons with spin up and spin down are the same. One can also see that the tunneling current in parallel configuration decreases more sharply than that in antiparallel configuration with P increasing, and when $P = 0.8$, the magnitude of the tunneling current in parallel configuration is much lower than that in antiparallel configuration, as shown in Fig. 2(a). This result can be ascribed to the fact that the tunneling of electrons is affected more strongly by the polarization in parallel configuration. In our calculations, the sharp reduction of the total tunneling current is mostly given rise by the decrease of spin up current, which we have discussed in Fig. 3.

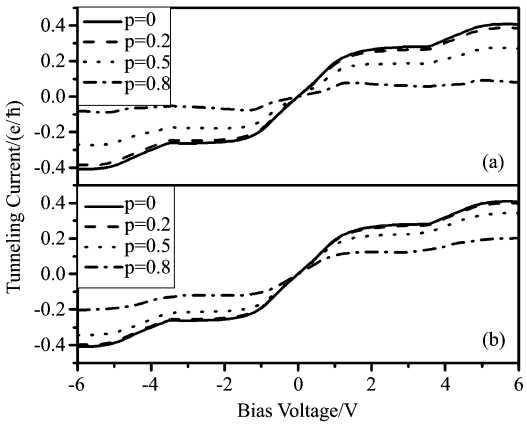

Fig. 2　Bias dependence of the tunneling current in parallel (a) and antiparallel (b) configuration. $P_L = P_R = 0, 0.2, 0.5, 0.8$; Other parameters are $t_{d_1 d_2} = 0.8$; $\phi = \frac{\pi}{2}$; $\varepsilon_1 = \varepsilon_2 = 0$; $U = 2$; $k_B T = 0.01$

图 2　平行 (*a*) 与反平行 (*b*) 组态下的隧穿电流与电压关系图

In Fig. 3(a), it can be seen that, when $eV < -t_{d_1 d_2}$ and $eV > t_{d_1 d_2}$, the magnitude of spin up current is lower than that of spin down current. It means that spin polarized current appear in such situation. Meanwhile, the spin up and spin down current are almost the same when $-t_{d_1 d_2} < eV < t_{d_1 d_2}$. This characteristic is much different from that in antiparallel configuration, as shown in Fig. 3(b). One can see that, the magnitude of spin up current is much lower than that of spin down current at $eV < -t_{d_1 d_2}$, which is opposite to the case at $eV > t_{d_1 d_2}$, and the two curves almost overlap at $-t_{d_1 d_2} < eV < t_{d_1 d_2}$. These results indicate that spin polarized current can be obtained in our model system, especially at large bias voltage in parallel configuration, and this will be helpful to the generation of tunable spintronic devices.

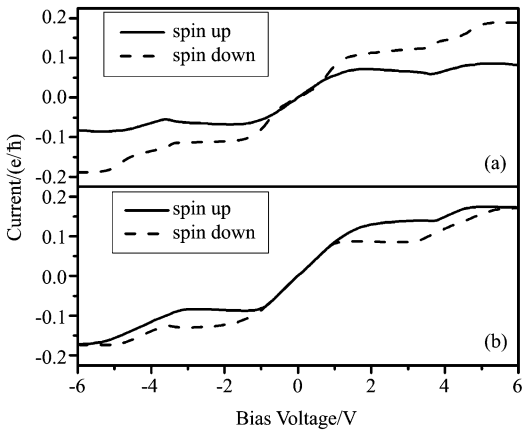

Fig. 3 Bias dependence of spin up and spin down current in parallel (a) and antiparallel (b) configuration. $P_L = P_R = 0.5$; $t_{d_1d_2} = 0.8$; $\phi = \frac{\pi}{2}$; $\varepsilon_1 = \varepsilon_2 = 0$; $U = 2$; $k_BT = 0.01$

图3 平行(*a*)与反平行(*b*)组态下的自旋向上电流与自旋向下电流与电压关系图

For all above results, the characteristics of tunneling current may be understood in terms of the total effective coupling strength $T_{\alpha d_i\sigma}$ between the leads and the two quantum dots. Suppose we split a beam of electrons that tunnel from QD1 to the left lead into two paths and then recombine them, one path is tunneling directly to the left lead, the other is traveling to QD2 first, then to the right lead and finally to the left lead passing through the upper arm of the ring. The case of electrons tunneling from QD1 to the right lead is that, one path is first traveling to the QD2, then to the right lead, the other is first tunneling to the left lead, then to the right lead passing through the upper arm, and the effective coupling strengths between QD2 and the two leads could be understood as the case of QD1. The total effective coupling strength $T_{\alpha d_1\sigma}$ can be described as

$$\begin{aligned} T_{Ld1\sigma} &= |\ t_{Ld1} + t_{LR}e^{-i\phi}(-i\pi\rho_{R\sigma})t_{Rd2}g^r_{d2d2}t_{d1d2}\ |^2 \\ &= |\ t_{Ld1}\ |^2 + |\ t_{LR}\pi\rho_{R\sigma}t_{Rd2}g^r_{d2d2}t_{d1d2}\ |^2 \\ &\quad - 2\pi\rho_{R\sigma}t\sin\phi \quad , \end{aligned} \tag{7}$$

$$\begin{aligned} T_{Rd1\sigma} &= |\ t_{Rd2}g^r_{d2d2}t_{d1d2}\ |^2 + t_{LR}e^{i\phi}(-i\pi\rho_{L\sigma})t_{Ld1}\ |^2 \\ &= |\ t_{Rd2}g^r_{d2d2}t_{d1d2}\ |^2 + |\ t_{LR}\pi\rho_{L\sigma}t_{Ld1}\ |^2 + 2\pi\rho_{L\sigma}t\sin\phi \quad , \end{aligned} \tag{8}$$

where $t = t_{Ld1}t_{Rd2}t_{LR}t_{d1d2}$, $\pi\rho_{L\sigma} = \frac{\Gamma_{L\sigma}}{2\ |\ t_{Ld1\sigma}\ |^2}$, $\pi\rho_{R\sigma} = \frac{\Gamma_{R\sigma}}{2\ |\ t_{Rd2\sigma}\ |^2}$. We can obtain the strengths of coupling between QD2 and the two leads in the same way. Due to the distinction of the total effective coupling strength between both quantum dots and the leads for each spin, the situation of tunneling through the two quantum dots for spin up and spin down electrons will be different. From Eq. (7) and (8), it can be found that the total effective coupling strength is associated with the polarization and magnetic configuration of the leads, and the behavior appearing in Fig. (2) and (3) can be understood from $T_{Ld1\sigma}$. Meanwhile, in Eq. (7), it also can be seen that the change of $\rho_{R\sigma}$ in the second term $|t_{LR}\pi\rho_{R\sigma}t_{Rd_2}g^r_{d_2d_2}t_{d_1d_2}|^2$ and the third term $2\pi\rho_{R\sigma}t\sin\phi$ leads to different coupling strength $T_{Ld_1\sigma}$, and the second term changes more slightly than the third term when tuning P. Consequently, both $T_{Ld1\uparrow}$ and $T_{Ld1\downarrow}$ decrease while increasing P in both configurations, which results in the reduction of the total tunneling current in Fig. 2. In addition, different spin component induce the distinction between $T_{Ld1\uparrow}$ and $T_{Ld1\downarrow}$. In Fig. 3(a), the magnitude of spin up current in parallel configuration is much lower than that of spin down current, which demonstrates that it is harder for spin up electrons to tunnel through QDs. In antiparallel configuration as shown in Fig. 3(b), it is harder for spin up electrons to travel under negative voltage bias.

We have also discussed the AB oscillations of the conductance in both configurations. Due to the interference between the two different paths, one of which is passing through double quantum dots and the other is along the direct channel, the AB oscillations appear in our system. The numerical results reveal that the magnetic flux could affect the tunneling properties of the electrons effectively, and the conductance changes with the magnetic flux ϕ periodically.

Fig. 4 presents the differential conductance versus the magnetic flux in one period. From this figure, one can see that, when $\phi = 0$ or $\phi = 2\pi$, the differential conductance reaches maximum, and when $\phi = \pi$, the conductance shows minimum, which means that the electric current will change more smoothly relative to the case for $\phi \neq \pi$. It can also be seen that, with the increase of P, the magnitude of the conductance decreases. By comparing the two different configurations, the conductance in antiparallel configuration (Fig. 4 (b)) decreases more sharply than that in parallel configura-

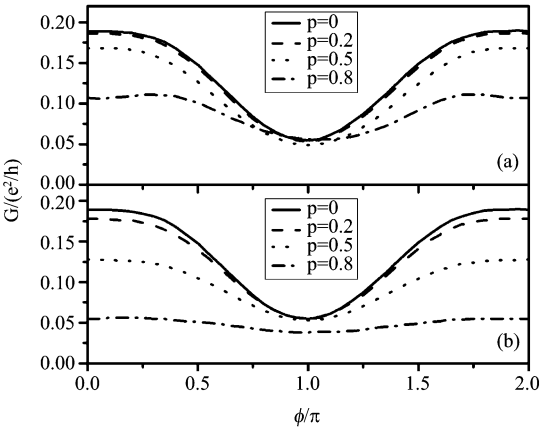

Fig. 4　Differential conductance versus the magnetic flux for four values of $P_L = P_R = 0, 0.2, 0.5, 0.8$ in parallel (a) and antiparallel (b) configuration. Other parameters are $t_{d_1d_2} = 0.8$; $\varepsilon_1 = \varepsilon_2 = 0$; $U = 2$; $k_BT = 0.01$

图 4　在 $P_L = P_R = 0, 0.2, 0.5, 0.8$ 的情况下，微分电导与磁通的关系图

tion (Fig. 4 (a)), and when $P = 0.8$, it changes slightly when tuning the magnetic flux.

The spin accumulation of both quantum dots in antiparallel configuration is also investigated, and the numerical result is given in Fig. 5. The appearing of spin accumulation can be ascribed to the difference between the electron incoming and outgoing rate for each QD, and the different coupling strengths make it easier for one spin to inject into a QD but harder to leave, or harder to inject but easier to leave.

Fig. 5 displays the bias dependence of the spin

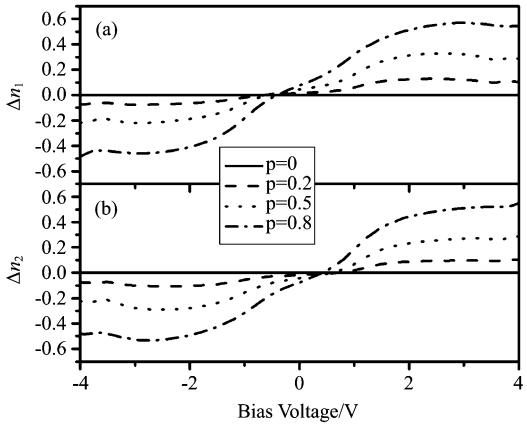

Fig. 5　Bias dependence of the spin accumulation on dot1 (a) and dot2 (b) in antiparallel configuration. $P_L = P_R = 0, 0.2, 0.5, 0.8$; $t_{d_1d_2} = 0.8$; $\phi = \frac{\pi}{2}$; $\varepsilon_1 = \varepsilon_2 = 0$; $U = 2$; $k_BT = 0.01$

图 5　量子点 1 (a) 与量子点 2 (b) 中的自旋累积与电压关系图

accumulation for different polarization in both quantum dots in antiparalle configuration. It can be seen that the characteristics of spin accumulation in QD1 and QD2 are almost similar. Moreover, the spin accumulation is affected strongly by polarization. When $P = 0$ no spin accumulation exist in both quantum dots. This is because the contribution of spin up electrons is the same as that of spin down electrons. With the increase of P, the spin accumulation increases in both quantum dots, which may have practical usage, such as to filter or store the electron spin in the QD. In addition, obvious spin accumulation can also be found in parallel configuration, and the spin accumulation effects in both configurations will lead to the decrease of the tunneling current, and may play an important role in magnetotransport properties.

3　Conclusions

In summary, the spin dependent transport through double quantum dots embedded in one arm of the A-B ring coupled to ferromagnetic leads has been studied by using nonequilibrium Green function method. At the given situation, the current decreases with P increasing. It is also found that the tunneling behaviors for spin up and spin down electrons are quite different in both configurations. These may result in the existence of spin polarized current for this model system. In addition, the interference between the path passing through the quantum dots and the direct path could be seen when tuning the magnetic flux. These results can be ascribed to that the polarization, the magnetic configuration and the magnetic flux may affect the total effective coupling strengths, which make it easier or harder for one spin to tunnel through this system. Meanwhile, different incoming and outgoing rate for each QD give rise to the spin accumulation, and with the increase of P, the spin accumulation increases obviously in antiparallel configuration, which leads to the decreases of tunneling current.

These results indicate that the spin polarized current can be obtained in our model system, and may be helpful to the generation of tunable spintronic devices. In addition, the large spin accumulation may be of practical use in quantum information storage.

(下转 112 页)

The experiment results and theoretical analysis indicate that our algorithm can eliminate stripe noise effectively and also can be completed in one frame time.

REFERENCES

[1] Ni C, Li Q, Xia L Z. A novel method of infrared image denoising and edge enhancement [J]. *Signal Processing*, 2008, **88**(6): 1606 - 1614.

[2] Vergara L, Bernabeu P. Automatic signal detection applied to fire control by infrared digital signal processing[J]. *Signal Processing*, 2000, **80**(4): 659 - 669.

[3] Hardie R C, Baxley F, Brys B, *et al.* Scene-based nonuniformity correction with reduced ghosting using a gated LMS algorithm [J]. *Optics Express*, 2009, **17** (17): 14918 - 14933.

[4] Leathers R, Downes T, Priest R. Scene-based nonuniformity corrections for optical and SWIR pushbroom sensors[J]. *Optics Express*, 2005, **13**(13): 5136 - 5150.

[5] Hardie R C, Hayat M M, Armstrong E Y, *et al.* Scene-based nonuniformity correction with video sequences and registration[J]. *Applied Optics*, 2000, **39**(8): 1241 - 1250.

[6] Narayanan B, Hardie R C, Muse R A. Scend-based nonuniformity correction technique that exploits knowledge of the focal-plane array readout architecture[J]. *Applied Optics*, 2005, **44**(17): 3482 - 3491.

[7] Harris J G, Chiang Y M. Nonuniformity correction of infrared image sequences using the constant-statistics constraint [J]. *IEEE Trans. Image Processing*, *IEEE Transactions on*, 1999, **8**(8): 1148 - 1151.

[8] Kim J H, Ahn S S, Kwon C H, *et al.* An output channel nonuniformity compensation driving method in flat panel display driving circuits[J]. *Display Technology*, 2006, **2**(4): 386 - 392.

[9] Cohen M, Cauwenberghs G. Floating-gate adaptation for focal-plane online nonuniformity correction[J]. *Circuits and Systems II: Analog and Digital Signal Processing*, *IEEE Transactions on*, 2001, **48**(1): 83 - 90.

[10] Hatle M, Vobecky J. Infrared observation of gate turn-off thyristor segment parameter nonuniformity [J]. *Electron Devices*, *IEEE Transactions on*, 1990, **37**(4): 1169 - 1171.

[11] Tabib-Azar M, Pathak P S, Ponchak G, *et al.* Nondestructive superresolution imaging of defects and nonuniformities in metals, semiconductors, dielectrics, composites, and plants using evanescent microwaves[J]. *Review of Scientific Instruments*, 1999, **70**(6): 2783 - 2792.

[12] Sui X B, Chen Q, Gu G H, *et al.* Research on the response model of microbolometer [J]. *Chin. Phys. B*, 2010, **19**(10): 108702-1-10.

[13] Wang B J, Liu S Q, Bai L P. An enhanced non-uniformity correction algorithm for IRFPA based on neural networkwork[J]. *Optics Communications*, 2008, **281** (8): 2040 - 2045.

[14] Wang B J, Liu S Q, Lai R. Adaptive non-uniformity correction algorithm for IRFPA based on neural networkwork [J]. *J. Infrared Milim Waves*, 2006, **25**(6): 405 - 407.

[15] Przelaskowski A, Jóźwiak R, Krzyżewski T, *et al.* Ordering of diagnostic information in encoded medical images [J]. *Accuracy progression*, *Image Processing Technology*, 2008, **16**(1): 49 - 59.

[16] SM320DM642-EP Video/imaging fixed point digital signal processor. USA: Ti corporation (2007).

(上接101页)

REFERENCES

[1] Zhu J X, Balatsky A V. Josephson current in the presence of a precessing spin [J]. *Phys. Rev. B*, 2003, **67** (17): 174505.

[2] Sun Q F, Zhu Y, Lin T H. Writing spin in a quantum dot with ferromagnetic and superconducting electrodes [J]. *Phys. Rev. B*, 2004, **69**(12): 121302.

[3] Kobayashi K, Aikawa H, Katsumoto S, *et al.* Tuning of the Fano effect through a quantum dot in an Aharonov-Bohm interferometer[J]. *Phys. Rev. Lett.*, 2002, **88**(25): 256806.

[4] Domanski T, Donabidowicz A, Wysokinski K I. Meservey-Tedrow-Fulde effect in a quantum dot embedded between metallic and superconducting electrodes [J]. *Phys. Rev. B*, 2008, **78**(14): 144515.

[5] Stefanski P. Proposal for a correlation induced spin-current polarizer[J]. *Phys. Rev. B*, 2008, **77**(12): 125331.

[6] Sergueev N, Sun Q F, Guo H, *et al.* Spin-polarized transport through a quantum dot: Anderson model with on-site Coulomb repulsion [J]. *Phys. Rev. B*, 2002, **65** (16): 165303.

[7] Ma J, Dong B, Lei X L. Quantum transport through double-dot Aharonov-Bohm interferometry in Coulomb blockade regime[J]. *Eur. Phys. J. B*, 2003, **36**(4): 599 - 605.

[8] Dong B, Djuric I, Cui H L, *et al.* Time-dependent resonant tunneling for parallel-coupled double quantum dots[J]. *J. Phys. Condens. Matter*, 2004, **16**(24): 4303 - 4314.

[9] Dong B, Lei X L, Horing N J M. First-order coherent resonant tunneling through an interacting coupled-quantum-dot interferometer: Generic quantum rate equations and current noise[J]. *Phys. Rev. B*, 2008, **77**(8): 085309.

[10] Chi F, Zheng J, Sun L L. Spin accumulation and pure spin current in a three-terminal quantum dot ring with Rashba spin-orbit effect[J]. *J. Appl. Phys.*, 2008, **104** (4): 043707.

[11] Ying Y B, Jin G J, Ma Y Q. Spin-polarized transport through an Aharonov-Bohm interferometer embedded with a quantum dot molecule [J]. *J. Phys. Condens. Matter*, 2009, **21**(27): 275801.